ARCHIVES OF ELECTRICAL ENGINEERING VOL. 65(4), pp. 827-841 (2016)

DOI 10.1515/aee-2016-0058

A closed-loop power controller model of series-resonant-inverter-fitted induction heating system

PALASH PAL[1], DEBABRATA ROY[2], AVIK DATTA[1], PRADIP K. SADHU[3], ATANU BANERJEE[4]

[1]*Department of Electrical Engineering*
Saroj Mohan Institute of Technology, Degree Engineering Division
Guptipara, Hooghly-712512, West Bengal, India

[2]*Department of Electrical Engineering*
Batanagar Institute of Engineering, Management & Science, A unit of Techno India™ Group
B7-360 / New,Ward No. 30, Putkhali, Maheshtala, Kolkata-700141,West Bengal, India

[3]*Department of Electrical Engineering*
Indian Institute of Technology, Indian School of Mines, Dhanbad
(Under Mhrd, Govt. Of India)
Dhanbad-826004, Jharkhand, India

[4]*Department of Electrical Eng.*
National Institute of Technology, Meghalaya
An Institute of National Importance under MHRD, Govt. of India
Bijni Complex, Laitumkhrah, Shillong-793003
Meghalaya, India

e-mail : debabrataroy1985@gmail.com

(Received: 07.07.2016, revised: 14.10.2016)

Abstract: This paper presents a mathematical model of a power controller for a high-frequency induction heating system based on a modified half-bridge series resonant inverter. The output real power is precise over the heating coil, and this real power is processed as a feedback signal that contends a closed-loop topology with a proportional-integral-derivative controller. This technique enables both control of the closed-loop power and determination of the stability of the high-frequency inverter. Unlike the topologies of existing power controllers, the proposed topology enables direct control of the real power of the high-frequency inverter.

Key words: induction heating, power controller, PID, series resonant inverter, MATLAB

1. Introduction

In a high-frequency induction heating process, the objects being heated are isolated from the heat source. An induction heater is used as a high-frequency electrical device for heating electrically conductive materials. A power electronic inverter circuit is incorporated in the de-

vice for generating high-frequency electricity. Because the heating process is contactless, high-frequency induction heating does not have any adverse effect on the material being heated. The induction heater is precise, environment friendly, energy efficient, and controllable; moreover, it enables rapid heating and can be repeatedly used. In particular, the heat is generated within the material being heated, resulting in negligible heat loss. By contrast, in other heating methods, heat is transferred from the heat source to the material being heated. Accordingly, high-frequency induction heating has unique industrial, domestic, and medical applications [1-3], and it is used in a wide range of fields. Currently, operations such as induction bonding, brazing, welding, forging, melting, and hardening can be achieved through high-frequency induction heating. This technique also creates the latest paradigm for biomedical electronics, and it can be employed for blood reheating during open heart surgery [4].

The use of high-frequency induction heating equipment is likely to increase rapidly in the near future [5]. The high-frequency induction heating equipment requires latest regulations and recommendations for future development. Moreover, innovative practical approaches should be developed for improving the quality of the input power supply of the induction heating equipment. High-frequency switching distorts the grid voltage, resulting in poor power quality [6].

The inverter has a problem when it is in a permanent resonant state: since it is quite easy to increase the pressure in the components towards the saturation value, the inverter can be damaged. It is necessary to introduce a control circuit to overcome this undesirable situation. Such a control circuit can control the response of the inverter when the inverter is constantly operated in a permanent resonant state [8–10].

In high-frequency inverters in a permanent resonant state a specific technique is commonly used for controlling the voltage and current supply with the desired signal error. However, the technique, which is shown in Fig. 1, has some demerits because it involves a large number of power semiconductors, driver parameters, and an extra control loop.

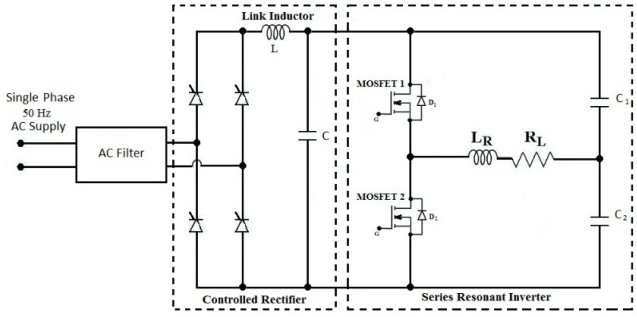

Fig. 1. Modified high-frequency half-bridge series resonant inverter with regimented DC supply

The system can be controlled using a self-adaptive loop and must have an operating frequency slightly greater than the resonant frequency of the tank circuit, which comprises an induction-coil-heated piece in series with a resonant capacitor. The high-frequency induction heating inductor current can be controlled by adjusting either the output current or output

voltage of the inverter, and the high-frequency control loop is sufficient to control these two output parameters [11-16].

A proportional-integral-derivative (PID) controller can give favourable results in induction heating applications. After designing a PID controller and corresponding incorporating PID controller in high-frequency application it is seen that this controller will be more suitable in high-frequency domain. The rated feedback can be obtained because the forward path gains are adjustable for the most suitable result of stability analysis.

2. High-frequency induction heating system

The high-frequency induction heating process consists of two major stages. First a diode bridge rectifier rectifies the AC supply signal, and subsequently, the rectified output is fed to a high-frequency inverter. An alternating magnetic field is produced by the high-frequency current at the inverter output, resulting in an eddy current being induced. This eddy current is responsible for generating heat at the surface of the object being heated. The internal resistance of the object is a vital parameter as it plays a role in heat generation through Joule heating [17, 18]. A block diagram of a modified DC-link high-frequency half-bridge series resonant inverter is shown in Fig. 2.

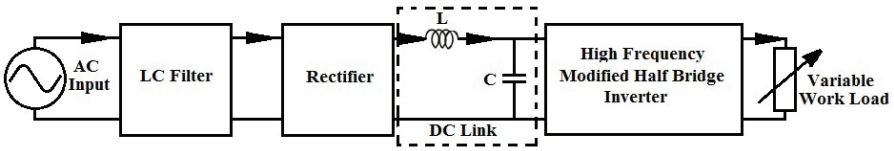

Fig. 2. Block diagram of the modified DC-link high-frequency half-bridge current source inverter

Generally, high-frequency induction heating involves an alternating magnetic field and the skin effect. The production of a high-frequency alternating magnetic field in the working coil generates heat and converts electrical energy to heat energy, which is intended at the skin depth as AC resistance is decreased [7].

3. Proposed modified half-bridge series resonant inverter

The modified half-bridge inverter circuit is normally designed for providing a moderate output power. Fig. 3 depicts the circuit diagram of the proposed modified half-bridge series resonant inverter. Two power semiconductor switches, such as MOSFETs, are used to trigger. Antiparallel diodes are connected to the switch that allows a current to flow when the main switch is turned OFF; the current flow results from the discharge of the inductor. If the inductor does not discharge, then it will not operate properly. The modified half-bridge series resonant inverter consists of two MOSFETs, a load resistance (R), and a load inductance (L);

L is the working coil used for high-frequency heating. A high power output can be achieved at a high switching frequency.

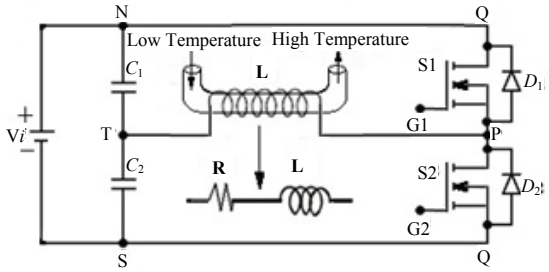

Fig. 3. Induction heating system based on the proposed modified half-bridge series resonant inverter

Table 1. Switching table of MOSFETs

S1	S2	V_{out}
ON	OFF	$+V_i/2$
OFF	ON	$-V_i/2$

Table 1 shows the switching operation of MOSFETs. In this study, MOSFETs were used as solid state switches because they are suitable for high-frequency operations. In Fig. 3, antiparallel diodes D_1 and D_2, which are connected to the switches S1 and S2 respectively, allow a current to flow when the main switch is turned OFF. When there is no signal at S1 and S2, capacitors C_1 and C_2 are charged such that each of the capacitors has a voltage of $V_i/2$. A gate pulse appears at the gate G and turns S1 ON. Capacitor C_1 discharges through the path NOPTN, and simultaneously, capacitor C_2 charges through the path NOPTS. Fig. 4 shows the direction of current flow through an induction heating system based on the modified half-bridge series resonant inverter, when S1 is turned ON. When S1 is turned OFF, the inductor starts discharging through the path PTSQ. Fig. 5 shows the discharging path. Furthermore, the discharging current of C_1 and the charging current of C_2 simultaneously flow from P to T.

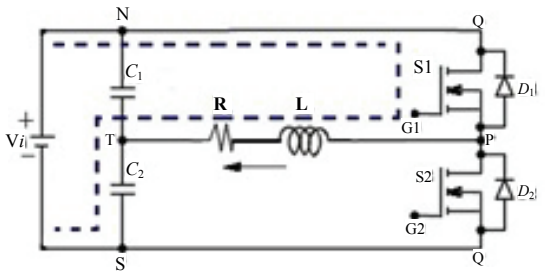

Fig. 4. Current flow diagram of the induction heating system based on the modified half-bridge series resonant inverter, when S1 is turned ON

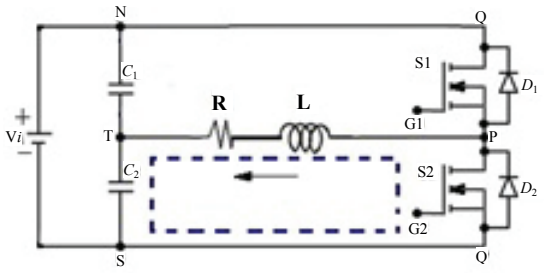

Fig. 5. Discharging path of the inductor when S1 is turned OFF

In the next slit of the gate pulse, S1 and S2 are in the OFF state, and each of the capacitors is again charged to a voltage of *Vi*/2. A gate pulse appears at the gate G to turn ON the switch S2. Furthermore, the capacitor C_2 discharges through the path TPQST, and the charging path for capacitor C_1 is NTPQS. The discharging current of C_2 and the charging current of C_1 simultaneously flow from *T* to *P*. Fig. 6 depicts the current flow diagram of the heating system based on the modified half-bridge series resonant inverter, when S2 is turned OFF, and Fig. 7 shows the discharging path of the inductor when S2 is turned OFF.

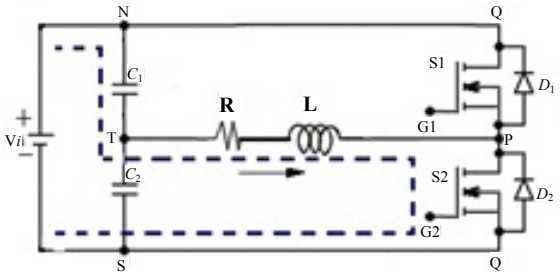

Fig. 6. Current flow diagram of the heating system based on the modified half-bridge series resonant inverter, when S2 is turned OFF

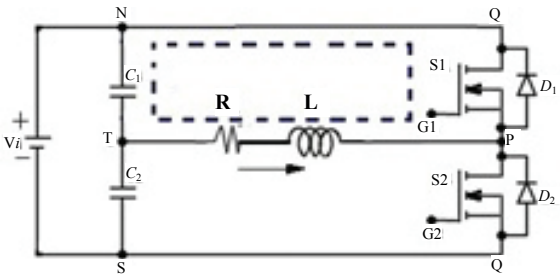

Fig. 7. Discharging path of the inductor when S2 is turned OFF

To prevent the voltage source from being short-circuited, the switches S1 and S2 must not operate simultaneously. For a resistive load, the current and voltage waveforms are in phase, unlike the case of a reactive load. Two freewheeling diodes offer discharging paths for the energised inductor. Fig. 8 depicts the output voltage waveform of the modified half-bridge series resonant inverter.

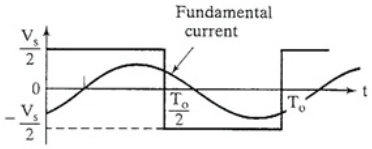

Fig. 8. Output voltage waveform of the modified half-bridge series resonant inverter

Sufficient heat is produced by the eddy current at high frequencies to the working coil. Resonance occurs when the inductor and capacitor exchange energy. The resonating components and switching devices of the modified half-bridge inverter are connected in series with the load for realising an underdamped circuit. Owing to the natural characteristics of the underdamped circuit, the current through the switching devices is zero. In voltage source inverters, two switches of an inverter leg cannot be turned on simultaneously since it can cause a short circuit. The time interval between the turning off of a switch and the turning on of the other switch is called dead time. In this methodology, antiparallel diodes are used in the induction heating system to facilitate freewheeling operation for allowing the inductor to discharge when one of the switches is in the OFF state.

4. Description of block diagram of proposed closed-loop induction heating system

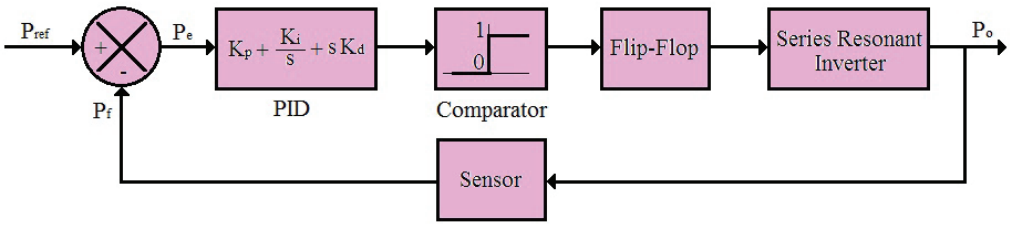

Fig. 9. Block diagram of the proposed closed-loop induction heating system

Figure 9 presents a block diagram of the proposed closed-loop induction heating system with a PID controller. The PID controller output is directly provided to the comparator. The comparator output is 0 (1) when the PID controller output is greater (lesser) than 0. The comparator output is recorded by the flip-flop. Furthermore, the flip-flop output is connected to a load with zero-crossing current that observed the system in a permanent resonant state. The sensor provides a feedback signal to the input, and the power error can be analysed. The most significant blocks are the sensor, PID controller, and load circuit, and the others blocks likely constant block can be incorporated in the total system response.

The overall transfer function can be obtained from the block diagram of the proposed closed-loop induction heating system, and the overall system response for high-frequency induction heating can be determined. Owing to the addition of the PID controller, the inverter

response will be very fast, and the inverter can be operated in a permanent resonant state without any problem. The definition of the variables and the significance of the blocks in Fig. 9 are as follows: P_{ref} is the reference power, P_e is the difference between the output power and the input power (i.e., error in the power), P_f is the power of the feedback signal, P_o is the output power, the PID block is a compensator network, the comparator and flip-flop blocks are synchronous delta generators, and the sensor block is a real power measurement system; the series resonant inverter (SRI) is also referred to as power stage model and comprises a power switch, load circuit, and power supply.

Figure 10 shows the PID compensator circuit diagram with the classic analogue topology. The circuit can be mathematically expressed as

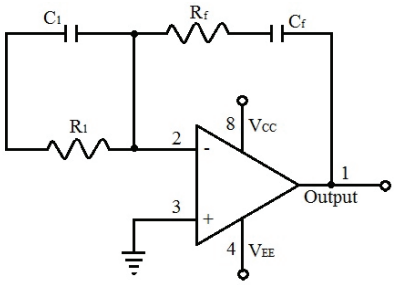

Fig. 10. PID compensator circuit diagram

$$\frac{\boldsymbol{V_o(s)}}{\boldsymbol{V(s)_i}} = \frac{(\boldsymbol{sR_fC_f}+1)\ (\boldsymbol{sR_1C_1}+1)}{\boldsymbol{sR_1C_1}+1}.$$

This system can be tuned by changing the parameters.

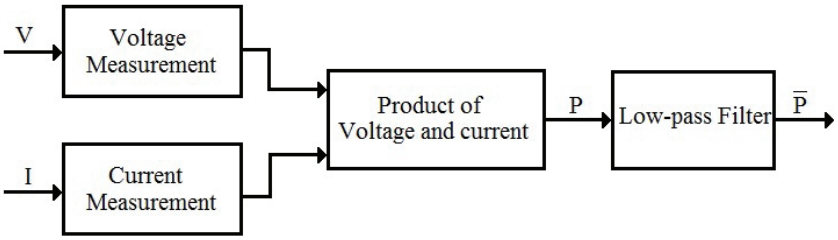

Fig. 11. Block diagram of the power sensor

Fig. 11 shows a block diagram of the power sensor. The power equation is given by

$$P = \frac{V_{\text{out}}I_{\text{out}}}{2}\sin(2\omega t - \phi) + \frac{V_{\text{out}}I_{\text{out}}}{2}\sin(\phi)$$

and the output of the low-pass filter is given by

$$\overline{P} = \frac{V_{\text{out}} I_{\text{out}}}{2} \sin(\phi) \approx \frac{V_{\text{out}} I_{\text{out}}}{2} (\phi) .$$

The overall transfer function of the power sensor can be obtained after the filter is designed, and it is given by

$$P_{\text{sensor}}(s) = \frac{xs^2 - ys + z}{as^4 + bs^3 + cs^2 + ds + e},$$

where x, y, z, a, b, c, d, and e are the coefficients of the order of the transfer function.

For high-power switches, an activator is required. The flip-flop is a type of activator whose output can be used for managing the driver and activating the high-power switches. The flip-flop does not influence the shape of the transfer function, and it is used to develop the structure of the closed-loop controller only for regulating the output power.

5. Load circuit model

In this context, Fig. 12 presents the equivalent circuit of the induction heating system; L_1 denotes the coil self-inductance, L_2 is the load self-inductance, K is the mutual inductance between the load and the coil, R_L is the load resistance, V_i and V_o are the system voltages, and I_1 and I_2 are the system currents.

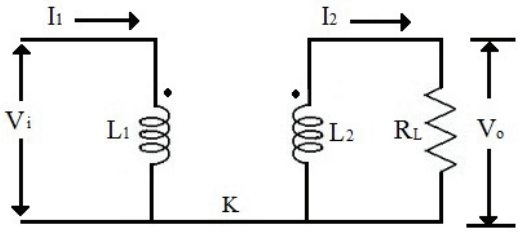

Fig. 12. Equivalent circuit of the induction heating system

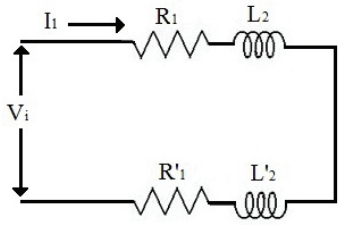

Fig. 13. Reduced equivalent circuit of the induction heating system

Figure 13 depicts reduced equivalent circuits of the working coil and load system of the induction heating system. In the figure, R_1 is the primary coil self-resistance, L_2 is the primary

coil self-inductance, R_1' is the value of the secondary resistance (R_{sec}) refers to the primary side, L_1' is the value of the secondary inductance (L_{sec}) refers to primary side.

The mathematical expression for the reduced equivalent circuit can be derived as follows by using Fig. 9:

$$V_i = j\omega L_1 I_1 - j\omega K I_2 , \tag{1}$$

$$V_o = -j\omega K I_1 + j\omega L_{\text{sec}} I_2 . \tag{2}$$

On the basis of (2), I_2 can be written as a function of I_1:

$$I_2 = \frac{j\omega K}{R_{\text{sec}} + j\omega L_{\text{sec}}} I_1 , \tag{3}$$

where $R_{\text{sec}} = \dfrac{V_2}{I_2}$.

Using the value of I_2 in (1) gives

$$V_i = j\omega L_1 I_1 - j\omega K \left(\frac{j\omega K}{R_{\text{sec}} + j\omega L_{\text{sec}}} \right) I_1 ,$$

$$V_i = \left(j\omega L_1 + \frac{j\omega^2 K^2}{R_{\text{sec}} + j\omega L_{\text{sec}}} \right) I_1 . \tag{4}$$

Therefore, the impedance

$$Z\left(= \frac{V_1}{I_1} \right)$$

can be obtained from the primary side, and it is equivalent to a single non-coupled inductor L_1 cascaded with another inductor. In particular, the above expression can be written as

$$Z_R(j\omega) = \frac{\omega^2 K^2}{R_{\text{sec}} + j\omega L_{\text{sec}}} = \frac{\omega^2 K^2}{R_{\text{sec}} + j\omega L_{\text{sec}}} \cdot \frac{R_{\text{sec}} - j\omega L_{\text{sec}}}{R_{\text{sec}} - j\omega L_{\text{sec}}} = \frac{\omega^2 K^2 R_{\text{sec}} - j\omega^3 K^2 L_{\text{sec}}}{R_{\text{sec}}^2 + \omega^2 L_{\text{sec}}^2}$$
$$\frac{\omega^2 K^2 R_{\text{sec}}}{R_{\text{sec}}^2 + \omega^2 L_{\text{sec}}^2} - \frac{j\omega^3 K^2 L_{\text{sec}}}{R_{\text{sec}}^2 + \omega^2 L_{\text{sec}}^2} . \tag{5}$$

This expression has two parts: a real part and an imaginary part. The real part of the impedance represents the load resistance reflected by the primary side of the main coil, and the imaginary part reduces the total circuit inductance.

Since the reactive current component is nullified in resonant conditions, a resonant capacitor C is included in Fig. 14.

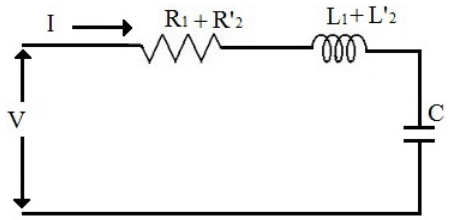

Fig. 14. Reduced equivalent circuit diagram of the induction heating system

The overall transfer function is given by

$$\frac{V_R(s)}{V_s} = \frac{s\dfrac{R}{L}}{(s+(a+j\omega))(s+(a-j\omega))} = \frac{s\dfrac{R}{L}}{((s+a)^2+\omega^2)}, \tag{6}$$

where

$$a = \frac{R}{2L} \quad \text{and} \quad j\omega = \sqrt{\frac{R^2}{2L} - \frac{1}{LC}}.$$

Again $R=R_1+R_2'$ and $L = L_1 + L_2'$.

As the system operates under resonant conditions, the voltage V is required on the primary side, and the voltage is identical to $V_1 \sin \omega t$. The inverse Laplace transform of (6) can be written as

$$V_R(t) = V_i \frac{2}{a^2+4\omega^2}\begin{bmatrix} a(1-\omega e^{-at})\cos\omega t \\ +(2\omega^2-(a^2+2\omega^2)e^{-at})\sin\omega t \end{bmatrix}. \tag{7}$$

The power dissipated in the load upon the application of a step voltage $V_i\, u(t)$ is given by

$$P(s) = \frac{V_i^2}{2R} M_1^2 \frac{(M_2^2-2M_2+1)s^2+(3-4M_2+M_2^2)as+2a^2}{s^3+3as^2+2a^2s}, \tag{8}$$

where

$$sP(s) = P_L(s),$$

$$M_1 = \frac{2(a+2\omega^2)}{(a^2+4\omega^2)},$$

$$M_2 = \frac{2(a^2+a\omega+2\omega^2)}{(a^2+2\omega^2)}.$$

The final power transfer function of induction heating can be expressed as

$$P_L(s) = \frac{V_i^2}{2R} M_1^2 \frac{(M_2^2 - 2M_2 + 1)s^2 + (3 - 4M_2 + M_2^2)as + 2a^2}{s^2 + 3as + 2a^2}. \tag{9}$$

6. Simulation results and discussion

For the proposed topology, all the required transfer functions were determined. The open-loop system behaviour allows changes in the positions of poles and zeros in the PID compensation network until a stable configuration is attained. Fig. 15 depicts the root locus diagram of the modified half-bridge SRI without a PID controller. Furthermore, Fig. 16 presents the open-loop pole-zero diagrams as well as the Bode plot for the same SRI, showing that the SRI is unstable.

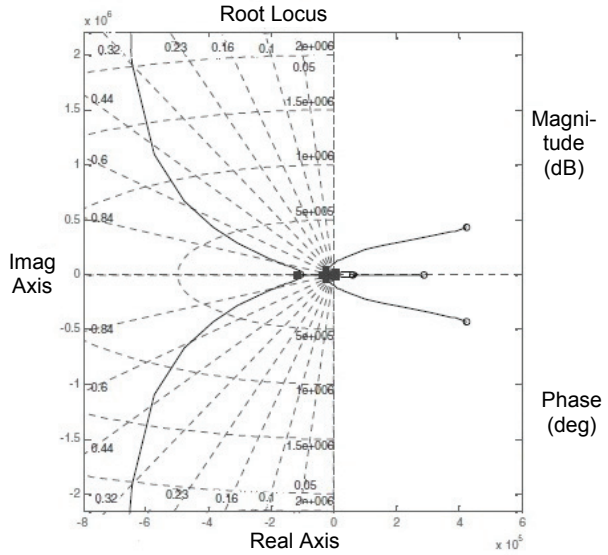

Fig. 15. Root locus diagram of the modified half-bridge SRI without a PID controller

After a PID controller is incorporated, the system can be easily and directly tuned by varying the PID parameters. The closed-loop behaviour of the system with the PID controller is shown in Fig. 17. Furthermore, Fig. 18 shows the closed-loop Bode plot diagram of the system, revealing a stable loop.

In Fig. 15, most of the open-loop poles are situated on the right-hand side of the *s*-plane, indicating that the system is unstable. However, after the PID controller was incorporated, because of the decrease in the system gain, all the poles shifted to the left-hand side of the *s*-plane (Fig. 17), reflecting a stable system.

Fig. 16 depicts the open-loop Bode plot diagram of the modified half-bridge SRI without a PID controller. The gain margin is −17.6 dB, and the phase margin is −90.7°.

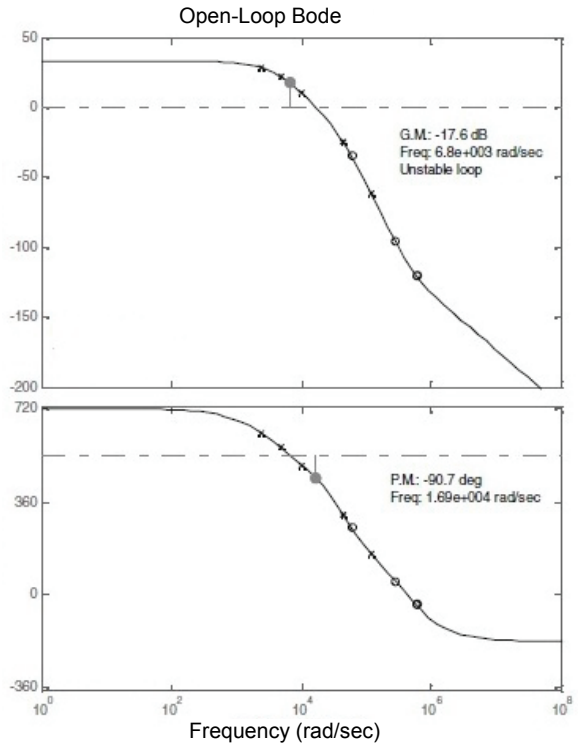

Fig. 16. Open-loop Bode plot diagram of the modified half-bridge SRI without a PID controller

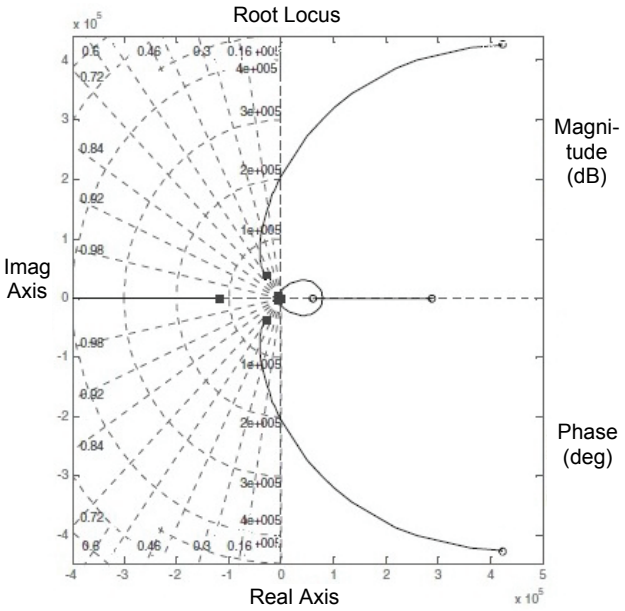

Fig. 17. Root locus diagram of modified half-bridge SRI incorporating a PID controller

By contrast, Fig. 18 presents the closed-loop Bode plot diagram of the modified half-bridge SRI incorporating a PID controller; the gain margin is 12.1 dB and the phase margin is 55.2°. Figs. 16 and 18 show different gain margins. The gain margin and phase margin in Fig. 16 are negative, whereas those in Fig. 18 are positive. Generally, positive values of the gain margin and phase margin indicate the safety margin for a stable system, and negative values for an open-loop system indicate an unstable system.

In Fig. 16, the phase crossover frequency is less than the gain crossover frequency, implying that the open-loop system is unstable. By contrast, in Fig. 18, the phase crossover frequency is greater than the gain crossover frequency, which is the condition for an unstable system.

The aforementioned results demonstrate that the addition of a PID controller critically influences the stability of the modified half-bridge SRI, and this concept can be used in applications of high-frequency induction heating.

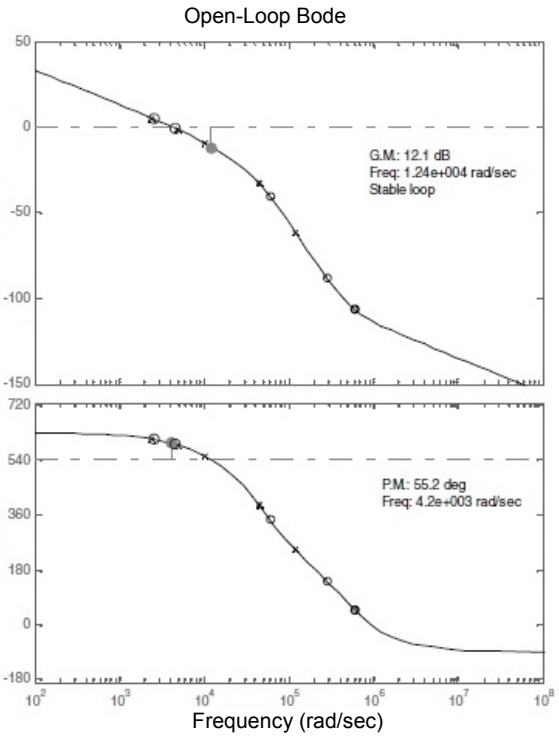

Fig. 18. Closed-loop Bode plot diagram of the modified half-bridge SRI incorporating a PID controller

7. Conclusions

In this paper, it is shown that a PID controller is the most important component of high-frequency induction heating equipment for achieving closed-loop power control. With the

small variation of the inverter circuit, the inverter may be uncontrolled. Furthermore, on the basis of the closed-loop system behaviour, it can be predicted that without a PID controller, the inverter will be unstable. So in this paper not only the closed-loop power is controlled, here the system behaviour may reach to stable condition. Furthermore, a control model is presented for achieving closed-loop power control in and the stable operation of a high-frequency inverter system.

References

[1] Sarnago H., Mediano L.A., Burdio J.M., *Class-D/DE dual mode-operation resonant converter for improved-efficiency domestic induction heating system*, IEEE Trans. Power Electronics, vol. 28, no. 3, pp. 1274-1285 (2013).

[2] Sarnago H., Gil L.O., Mediano A., M. Burdio J., *Modulation scheme for improved operation of an RB-IGBT-based resonant inverter applied to domestic induction heating*, IEEE Trans. Ind. Electron., vol. 60, no. 5, pp. 2066-2073 (2013).

[3] Sinha D., Sadhu P.K., Pal N., *Design of an Induction Heating Unit Used in Hyperthermia Treatment*, Advances in Therapeutic Engineering, CRC Press, Taylor & Francis Group, pp. 215-266 (2012).

[4] Pal P., Sadhu P.K., Pal N., Bhowmik P., *A New Heat Treatment Topology for Reheating of Blood Tissues after Open Heart Surgery*, Advancements of Medical Electronics, Springer India, pp. 101-108 (2015).

[5] York B., Yu W., Lai J.S., *Hybrid-frequency modulation for PWM integrated resonant converters*, IEEE Trans. Power Electronics, vol. 28, no. 2, pp. 985-994 (2013).

[6] Sadhu P.K., N. Pal, P. Pal, Sanyal S., *Selection of power semiconductor switches in modified half bridge resonant inverter fitted induction heater in power line for less harmonic injection*, International Journal of Power Electronics and Drive Systems, vol. 6, no. 1, pp. 121-128 (2015).

[7] Sadhu P.K., Pal N., Bhattacharya A., *Design of Working Coil Using Litz Wire for Industrial Induction Heater*, Lap Lambert Academic Publishing, ISBN: 978-3-659-35853-1, pp. 1-65 (2013).

[8] Espi J.M., Navarro A.E., Maicas J. et al., *Control circuit design of the L-LC resonant inverter for induction heating*, Power Electronics Specialists Conference, IEEE 31st Annual, vol. 3, pp. 1430-1435 (2000).

[9] Bolsens B., De Brabandere K., Van den Keybus J. et al., *Model-based generation of low distortion currents in grid coupled PWM-inverters using an LCL output filter*, IEEE Trans. Power Electronics, vol. 2, pp. 1032-1040 (2006).

[10] Pham H.N., Fujita H., Ozaki K., Uchida N., *Estimating method of heat distribution using 3-D resistance matrix for zone-control induction heating systems*, IEEE Trans. Power Electronics, vol. 27, no. 7, pp. 3374-3382 (2012).

[11] Mohanta D.K., Sadhu P.K., Chakrabarti R., *Fuzzy Markov model for determination of fuzzy state probabilities of generating units including the effect of maintenance scheduling*, IEEE Transactions on Power Systems, vol. 20, no. 4, pp. 2117-2124 (2005).

[12] Navarro D., Lucía O., Barragán L.A., Artigas J.I., Urriza I., Jiménez O., *Synchronous FPGA-based implementations of digital pulse width modulators*, IEEE Trans. Power Electronics, vol. 27, no. 5, pp. 2515-2525 (2012).

[13] Esteve V., Sanchis-Kilders E., Jordan J. et al., *Improving the efficiency of IGBT series resonant inverters using pulse density modulation*, IEEE Trans. Ind. Electron., vol. 58, no. 3, pp. 979-987 (2011).

[14] Khan I., Tapson J., De Vries I., *Frequency control of a current-fed inverter for induction heating*, Industrial Electronics, Proceedings of the 2000 IEEE International Symposium, vol. 1, pp. 343-346 (2000).

[15] Egalon J., Caux S., Maussion P., Souley M., Pateau O., *Multiphase system for metal disc induction heating: Modeling and RMS current control*, IEEE Trans. Ind. Appl., vol. 48, no. 5, pp. 1692-1699 (2012).

[16] Said A., Djamel B., Boudjema I., *Structural analysis for fault detection and isolation using the matching rank algorithm for residual generation: Application on an industrial water heating system*, Journal of Control Engineering and Applied Informatics, vol. 15, no. 2 (2013).
[17] Lucía O., Burdío J.M., Millán I., Acero J., Puyal D., *Load-adaptive control algorithm of half-bridge series resonant inverter for domestic induction heating*, IEEE Trans. Power Electronics, vol. 56, no. 8, pp. 3106-3116 (2009).
[18] Trentin A., Zanchetta P., Clare J., Wheeler P., *Automated optimal design of input filters for direct ac/ac matrix converters*, IEEE Trans. Ind. Electron., vol. 59, no. 7, pp. 2811-2823 (2012).